ARTICLE

Surfactant induced bilayer-micelle transition for emergence of functions in anisotropic hydrogel

Received 00th January 20xx,
Accepted 00th January 20xx

DOI: 10.1039/x0xx00000x

Md Anamul Haque[a,b], Takayuki Kurokawa[b,c], Tasuku Nakajima[b,c], Gen Kamita[d], Zannatul Fatema[a] and Jian Ping Gong[b,c,*]

Tuning the self-assembled structures in amorphous hydrogels will enrich the functionality of hydrogels. In this study, we tuned the structure of a photonic hydrogel, which consists of polymeric lamellar bilayers entrapped inside a polyacrylamide network, simply by molecular triggering using an ionic surfactant. Owing to the binding of ionic surfactants (sodium dodecyl sulfate), the lamellar bilayers comprising of non-ionic polymeric surfactants [poly(dodecyl glyceryl itaconate)] changed to micelles, whereas the unidirectional lamellar structure was preserved in the hydrogel. The bilayer-micelle structure transition caused a dramatic decrease in the swelling anisotropy and mechanical softening of the photonic gel. With the micelle structure, the softened gel shows fast (0.3 s) and reversible color change over the entire visible light range in response to a small mechanical pressure (5 kPa). This low stress-induced color-changing hydrogel could be applied as a visual tactile sensor in various fields, especially in biomedical engineering.

Introduction

Load-bearing soft bio-tissues and chemically synthesized hydrogels have been categorized to the same 'soft and wet' class of materials [1-3]. Hydrogels are three-dimensional cross-linked polymeric networks that are able to entrap large amounts of water in their matrix [4], and have been extensively considered as good candidates for the replacement of bio-tissues [1, 2]. However, whereas biological tissue displays various forms of functionality, hydrogels generally have poor functionality, primarily due to differences in their microstructures. Biological tissue possesses a well-defined hierarchical structure that endows living organisms with mechanical toughness and functionality in contrast to most conventional hydrogels, which are amorphous in their micro- and macro-scale structures [5-8]. Therefore, various attempts have been made to incorporate multiscale ordered and hierarchical structures into conventional amorphous hydrogels to bridge the gap between bio-tissue and hydrogels. Among the current strategies developed, self-assembly is a convenient and powerful method for incorporating ordered structures in the polymer network of hydrogels [9-16].

In recent years, numerous progress has been made in the development of self-assembled ordered structures in synthetic hydrogels through intermolecular interactions such as ionic bonding, hydrogen bonding, and hydrophobic interactions [5, 9, 11, 12]. These ordered structures endow the hydrogels with additional functionality and promising applications. Therefore, designing functional hydrogels with various ordered molecular structures and studying the resultant functionalities is an emerging area of research interest. However, once the ordered structures are formed by molecular self-assembly, they are frozen in hydrogels with irreversible functionalities [3, 16].

Being able to reversibly tune various properties of hydrogels is attractive for its potential application in materials science, such as in tissue engineering and mechano-optical sensors, and therefore is widely demanded. The properties of hydrogels are generally tuned by regulating their component mass fraction, crosslinking density, and molecular network conformation [17-24]. However, these strategies either permanently change the hydrogel networks or cannot be modified after hydrogel formation. Hence, tuning various properties of hydrogels by regulating the self-assembly structure is still limited [16, 25].

Recently, an anisotropic photonic hydrogel consisting of self-assembled lamellar bilayers entrapped inside a polymer network of polyacrylamide (PAAm) has been developed [26-28]. The bilayers are formed by the self-assembly of polymeric surfactant molecules, poly(dodecyl glyceryl itaconate) (PDGI). The bilayer PDGI/PAAm hydrogels had uniaxially aligned lamellar structures parallel to the sample surfaces. The periodic stacking of rigid, water-impermeable PDGI bilayers (4.7 nm-thick) into a soft PAAm hydrogel matrix (several hundred nanometers thick) [**Scheme 1, left column**] gives a perfect anisotropic structure integrated at the macroscopic scale. The PDGI bilayer membrane has a melting temperature of 43 °C [29]. At room temperature, a single bilayer is rigid, possessing a modulus on the order of several MPa, and the PAAm matrix is soft with a modulus of a few kPa [26,28]. Owing to the periodic

[a]*Department of Chemistry, University of Dhaka, Dhaka-1000, Bangladesh*
[b]*Faculty of Advanced Life Science, Hokkaido University, Sapporo 001-0021, Japan*
[c]*Institute for Chemical Reaction Design and Discovery (WPI-ICReDD), Hokkaido University, Sapporo 001-0021, Japan*
[d]*Graduate School of Life Science, Hokkaido University, Sapporo 001-0021, Japan*
**Corresponding Author, E-mail: gong@sci.hokudai.ac.jp*
Electronic Supplementary Information (ESI) available: [details of any supplementary information available should be included here]. See DOI: 10.1039/x0xx00000x

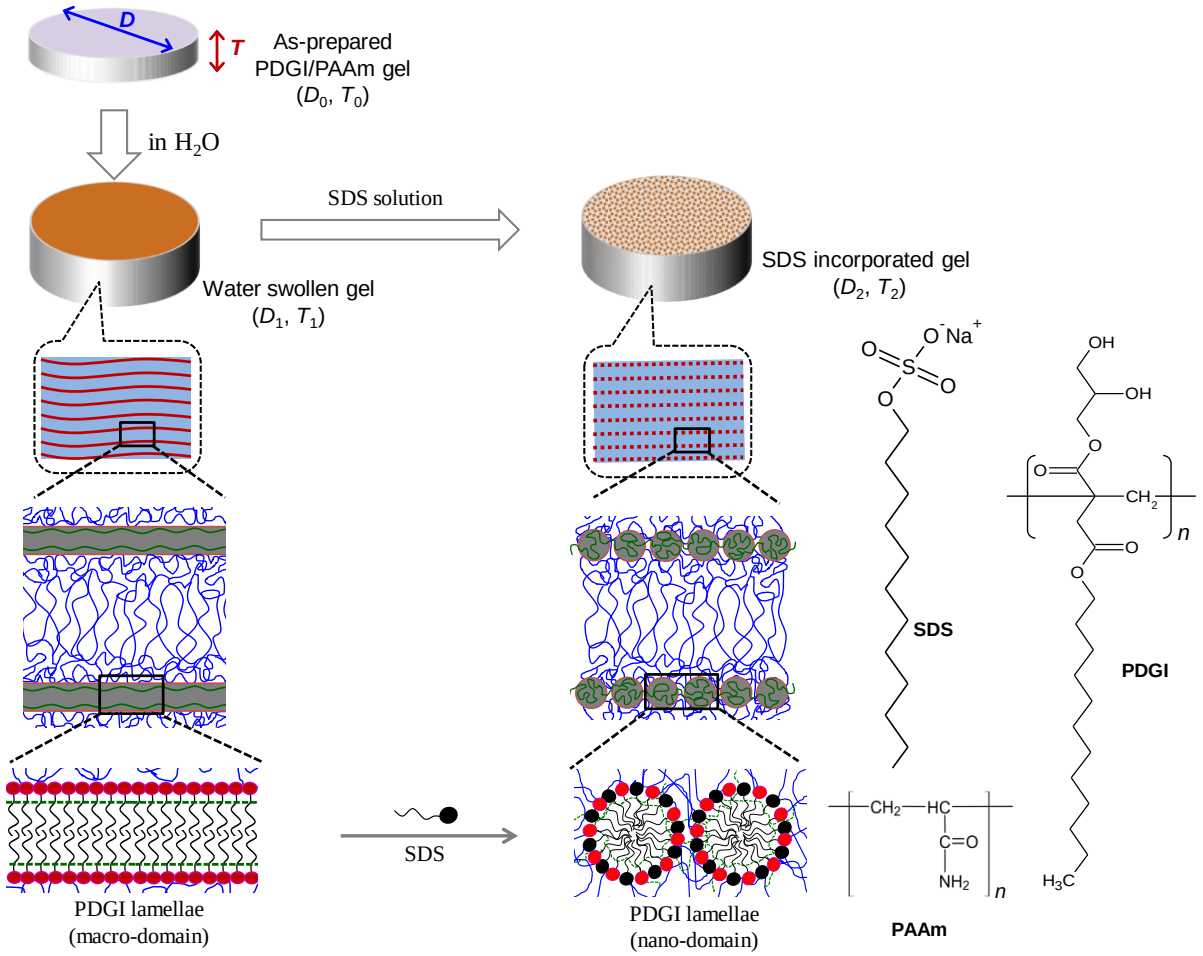

Scheme 1: Schematic of the structure change of PDGI/PAAm gel during the water swelling and surfactant binding. The as-prepared PDGI/PAAm gel (state 0) consisted of lamellar bilayers (~5 nm-thick) of self-assembled poly(dodecyl glyceryl itaconate) (PDGI) and polyacrylamide (PAAm) gel matrix (~250 nm-thick). Upon immersing in water, the gel swells only in the direction vertical to the water-impermeable bilayer (state 1). The water-swollen gel was then immersed in sodium dodecyl sulfate (SDS) aqueous solution for approximately a week to attain a new equilibrium (state 2). Disk shaped water swollen PDGI/PAAm hydrogel (left side) and the effect of SDS on the bilayer structure and bulk appearance of the hydrogel. Binding of SDS molecule to PDGI bilayer causes the breaking of bilayer and facilitates the formation of micelle above the critical micelle concentration (CMC) of SDS.

refractive index gradient, Bragg's reflection of visible light on the periodic lamellar plane causes the gel to exhibit excellent structural color, and the color can be tuned by various stimuli such as deformation, pH, and temperature [27, 34, 35]. The PDGI/PAAm lamellar hydrogels show many unique properties, including one-dimensional swelling in the thickness direction, anisotropic diffusion, and mechanical anisotropy [26-28,30-37]. Compared with the pure PAAm hydrogels, PDGI/PAAm lamellar hydrogels show significantly improved mechanical strength and toughness owing to the presence of macroscopic bilayers. For example, a PDGI/PAAm lamellar hydrogel containing only 5 mol% of dodecyl glyceryl itaconate (DGI) monomeric molecules relative to acrylamide (AAm) and occupying ~2% of gel volume, exhibited tensile fracture strength (~600 kPa), fracture strain (~20), and tearing resistance (~10 kJ/m^2), which are ~15, ~2, and ~1000 times greater than pure PAAm hydrogel, respectively [26,30,38]. For the PDGI/PAAm lamellar hydrogels, mechanical responses and the structural color can be tuned even after preparation by hydrolysis or polymerization with the addition of another component to the gels [33-35]. However, the process of adding the component and the subsequent chemical reaction is time-consuming, and the range of physical properties that can be tuned is not sufficient for wide potential applications.

In this work, using molecular triggering, we facilely tuned the self-assembled PDGI bilayer in the PAAm hydrogel matrix and investigated the effect of the modulated self-assembling structure on the properties of the hydrogel, including swelling, modulus, strength, toughness, and color tunability. For molecular triggering, we chose an ionic surfactant, sodium dodecyl sulfate (SDS), which possesses a similar hydrophobic tail as monomeric dodecyl glyceryl itaconate (DGI) molecules and can be incorporated into the PDGI bilayer assembly. In contrast to the non-ionic DGI molecules that form bilayers, the ionic SDS molecules form spherical micelles above the critical

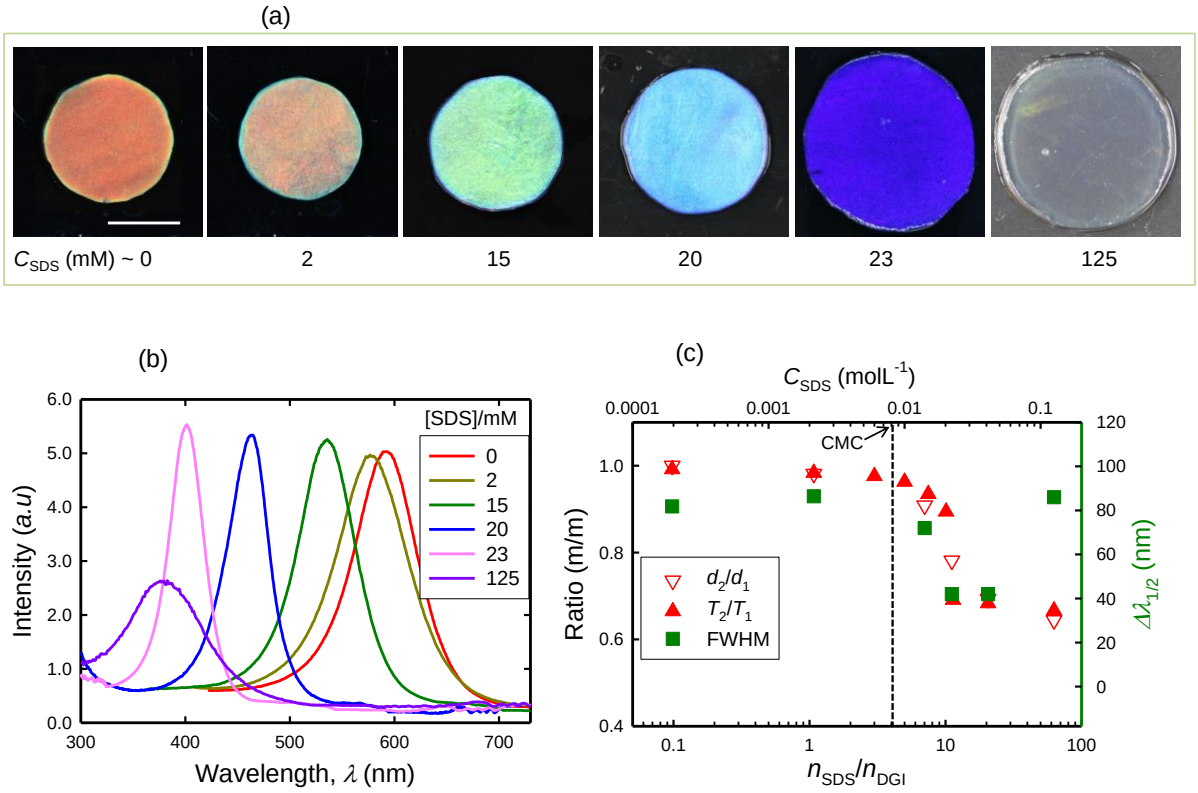

Figure 1: (a) Photographs of the disk-shaped PDGI/PAAm gel in water and in sodium dodecyl sulfate (SDS) solution of various concentrations. (b) Reflection spectra of gels in SDS solutions. (c) Inter bilayer spacing ratio (d_2/d_1), gel thickness ratio (T_2/T_1), and the full width at half maximum (FWHM, $\Delta\lambda_{1/2}$) in SDS solution of various concentrations. SDS concentrations are also expressed as the mole ratio to that of DGI in the gel (n_{SDS}/n_{DGI}). The scale bar in (a) is 5 mm. Subscripts 1 and 2 stand for the results in pure water and in SDS solution, respectively.

micelle concentration (CMC) because of the large volume ratio of the hydrophilic head to the hydrophobic tail [39,40]. The incorporation of a small amount of SDS in the PDGI bilayers increases the flexibility of the bilayers, whereas a large amount of SDS splits the macroscopic mono-domain PDGI bilayer sheets into smaller domains or even induces bilayer-micelle transition (**Scheme 1, right column**). Such structural changes dramatically change the properties of hydrogels. With the breaking of the bilayer into smaller domains or even micelles, the PDGI/PAAm gel becomes less anisotropic in swelling. The mechanical strength and toughness of the gel returned to the level of the soft and weak PAAm gel. Although SDS breaks the bilayers into small micelle-like domains, the PDGI assembly retains its layered structure, showing intense and brilliant structural color. The bilayer PDGI/PAAm gel undergoes a slow reversible response (~5 min) and full visible color switching at a relatively high pressure of approximately 60 kPa, whereas the micellar PDGI/PAAm gel undergoes an ultrafast response (0.3 s) with full visible color switching at a very small pressure of approximately 5 kPa. Photonic hydrogels functioning over a wide range of touch/pressure will find applications as visual stress sensors in various fields, especially in biomedical engineering.

Results and discussion

PDGI/PAAm gels with a monodomain lamellar bilayer structure were first immersed in water until swelling equilibrium was reached. The gels in this state are called non-treated gels. The non-treated gels were then soaked in SDS aqueous solutions of various concentrations (C_{SDS}) until equilibrium was reached. The gels that have been soaked in SDS solutions are called SDS-treated gels. Photographs of the non-treated gel and the SDS-treated gels with various SDS concentrations are shown in **Figure 1a**. At low SDS concentrations, the color of the gels remained nearly unchanged. Above the CMC, the color of the gels gradually changed from orange-red to transparent (ultraviolet) with increasing SDS concentration. The reflection spectra of the gels at various C_{SDS} values are shown in **Figure 1b**. The inter-bilayer distance (d) was calculated from the wavelength of maximum intensity (λ_{max}) using Bragg's equation. d initially remained unchanged at low C_{SDS} of ~260 nm but decreased with increasing SDS concentration (C_{SDS} > CMC), which is consistent with the blue shift in gel color (**Figure 1c**). d-spacing saturated to a value of ~150 nm at high SDS concentration (C_{SDS} > 23 mM). The full width at half maximum (FWHM, $\Delta\psi_{1/2}$) was estimated from the reflection spectra. The FWHM relative to that in water ($\Delta\psi_{1/2}/\Delta\psi_{1/2,0}$) decreased with increasing SDS concentration, except for a very high C_{SDS}, indicating that the lamellar periodic correlation is improved at high SDS concentrations. Along with the blue shift in color, the

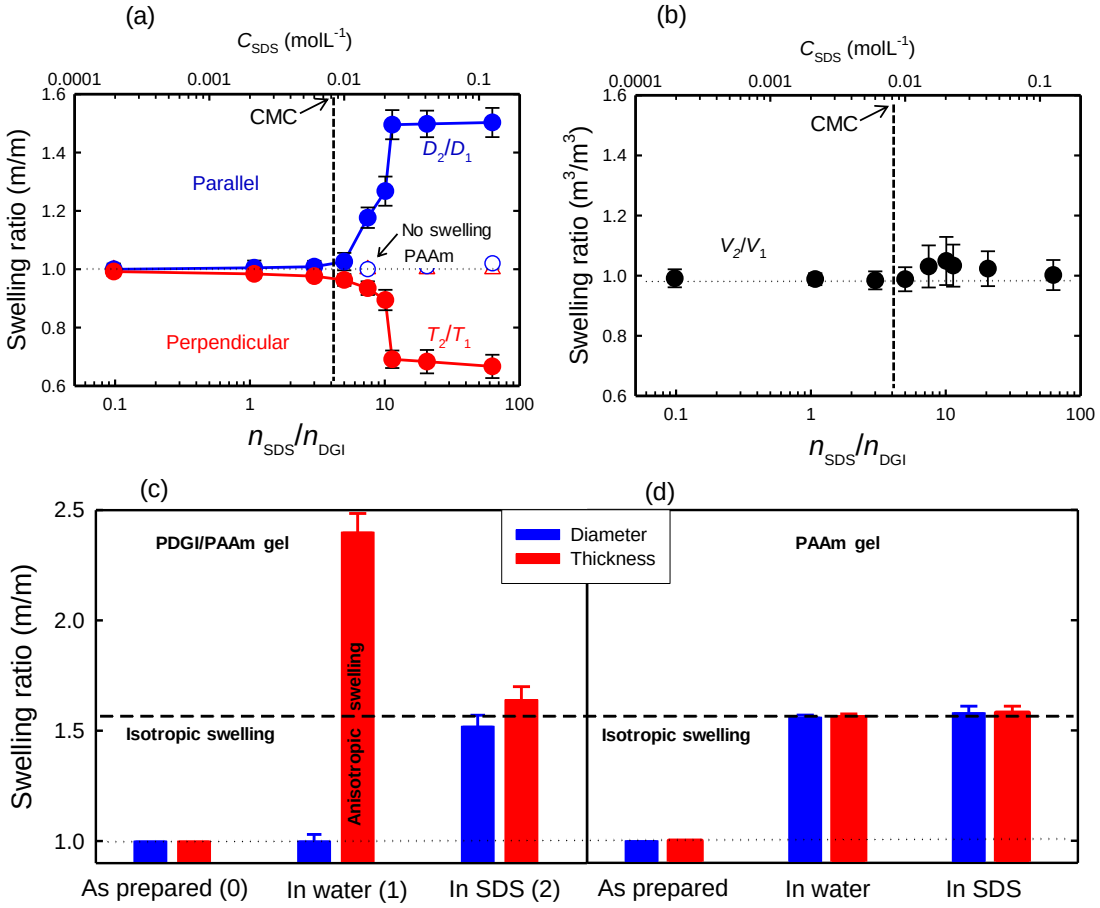

Figure 2: (a) Swelling ratios of the PDGI/PAAm gel in SDS solution (D_2/D_1, T_2/T_1). (b) Volume ratio of the PDGI/PAAm gel in SDS solution (V_2/V_1). (c) Swelling ratios of the PDGI/PAAm gel and PAAm gel in water (state 1) and in SDS solution (n_{SDS}/n_{DGI} >10) (state 2) relative to the as-prepared state (state 0). Subscript 0, 1, and 2 stands for the results at as-prepared state, in pure water, and in SDS solution, respectively. The vertical dotted lines in (a) and (b) are the critical micelle concentration (CMC) of SDS.

diameter of the gels apparently increased with the increase in SDS concentration, as observed from the photographs of the gel. As a control experiment, the gel does not exhibit such color and diameter change in NaCl solution (1 to 100 mM) within the concentration range of SDS used (**Figure S1**). We assumed primarily that SDS is incorporated in the PDGI bilayer and therefore induces structural change of the bilayers. Subsequently, changes in the diameter D, thickness T, and volume V of the PDGI/PAAm gels were investigated. First, the diameter (D_2/D_1) and thickness (T_2/T_1) of the SDS-treated gel relative to those of the non-treated gel were plotted as a function of the in-feed SDS concentration (**Figure 2a**). Here, the subscripts 1 and 2 of D and T denote the quantity of the gel equilibrated in water (non-treated gel) and equilibrated in SDS solutions (SDS-treated gel), respectively. SDS concentrations are also expressed as the mole ratio (in-feed) relative to that of DGI in the gel (n_{SDS}/n_{DGI}), as shown in the top x-axis. At low SDS concentrations, the diameter and thickness of the gel did not change but the thickness decreased sharply whereas the diameter increased at SDS ratios (n_{SDS}/n_{DGI}) above 7. Both the thickness and diameter saturated at very high SDS contents (n_{SDS}/n_{DGI} > 10). The change in thickness (T_2/T_1) agrees with the change in d-spacing (d_2/d_1) (**Figure 1c**). The increase in diameter was compensated by a decrease in thickness, and the gel maintained a constant volume (**Figure 2b**). The de-swelling in the direction perpendicular to the bilayer and swelling along the bilayer direction in the SDS solution originate from the anisotropic swelling of the non-treated PDGI/PAAm gel in water. The non-treated PDGI/PAAm gel showed perfect swelling anisotropy; it did not swell at all in the direction parallel to the bilayers (D_1/D_0 ~ 1) because the swelling is completely constrained by the water-impermeable and rigid nature of the uniaxially aligned, mono-domain PDGI bilayers (**Figure 2c**). Therefore, the gel only swelled in the thickness direction in water, perpendicular to the bilayer plane (T_1/T_0 ~ 2.4), owing to the free swelling of the PAAm matrix in the thickness direction. Here, the subscript 0 of D and T denotes the quantity of gel in the as-prepared state. Because a PAAm gel swells isotropically in water (T_1/T_0 = D_1/D_0 =1.6) (**Figure 2d**), the anisotropic swelling of PAAm layers confined between bilayers is energetically unfavorable. In the SDS solution (n_{SDS}/n_{DGI} > 10), the thickness of the gel decreased to T_2/T_0 ~ 1.62, whereas the diameter increased to D_2/D_0 ~ 1.55, which is very close to the isotropic swelling value of the PAAm gel (T_2/T_0 = D_2/D_0 =1.6)

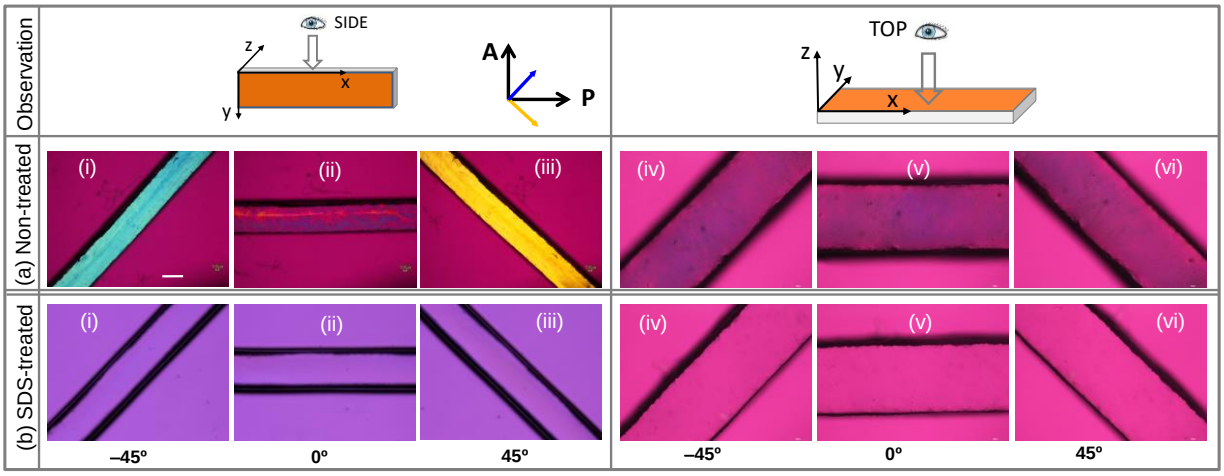

Figure 3: Polarizing optical microscope (POM) images of non-treated and SDS-treated (n_{SDS}/n_{DGI} ~ 60) PDGI/PAAm gels. The sample setup and observation directions are also shown. Scale bars are 1.0 mm.

(**Figure 2c, d**). No significant change in the swelling ratio was observed for the PAAm gel at high SDS concentrations (n_{SDS}/n_{DGI} > 10) (**Figure 2d**). These results indicate that at high SDS concentrations the mono-domain bilayer of the PDGI/PAAm gel is destroyed, and the gel swells isotropically, similar to the PAAm gel (**Figure S2**). To analyze the structural changes in the PDGI/PAAm gel, polarized optical microscope (POM) images of non-treated (or treated with low SDS) and treated (high SDS) PDGI/PAAm gels were captured and are shown in **Figure 3**. The sample setup and observation directions are also presented. All images were taken under cross polarizers in the presence of a tint plate (530 nm). The birefringence of the samples was assigned to uniaxially aligned bilayers and elongated PAAm chains in the thickness direction owing to anisotropic swelling. As shown in **Figure 3a(i–iii)**, images of the cross-section of the gel sheet (side) appear blue at -45° (i), magenta at 0° (ii), and orange at +45° (iii) relative to the polarizer. This is mainly due to the anisotropic swelling (deformation) of the PAAm matrix along the thickness direction and the uniaxially aligned lamellar bilayers parallel to the surface of the sheet-shaped gel. Top-view POM images of the gel showed negligible changes in birefringence color when the sample stage was rotated (-45° to 0° to +45°), confirming that the lamellar bilayers are isotropic in-plane (**Figure 3a(iv–vi)**). As shown in **Figure 3b(i–vi)**, images taken for both the cross-section (side) and top view for the PDGI/PAAm gel treated in highly concentrated SDS solution (n_{SDS}/n_{DGI} ~ 60) show no birefringence color at any rotation, as mentioned above. This clearly indicates that the PDGI bilayer assembly of the gel is damaged at high SDS concentrations, and the anisotropic PAAm matrix becomes isotropic.

The change in the bilayer structure can be correlated with the swelling of the gel in the SDS solution. At low concentrations of SDS (n_{SDS}/n_{DGI} < 5), SDS could hardly bind to PDGI, and the bilayer structure remained intact. Therefore, the gels maintained anisotropic swelling. However, at n_{SDS}/n_{DGI} > 5, massive SDS molecules could bind to the PDGI bilayers and break the bilayer mono-domain into smaller domains. This results in swelling along the diameter direction because the PAAm hydrogel layer favors isotropic swelling. At high SDS concentrations (n_{SDS}/n_{DGI} > 10), with excess binding of SDS to PDGI, bilayers split into nanoscale micelle-like domains, which allows the PAAm layer to swell freely along the diameter direction. The release of the constraint along the diameter allows PAAm to shrink along the thickness direction. As a result, the treated PDGI/PAAm gel attains an isotropic swelling at high SDS content, similar to the treated/non-treated PAAm gel.

The breaking of uni-domain bilayers into smaller domains or micelles significantly changes the mechanical properties of the gel. Stress-strain (s-s) profiles for the treated PDGI/PAAm gel are shown in **Figure 4a**. The stress–strain curve for the PAAm gel is also shown for comparison. At low SDS, the PDGI/PAAm gel with uni-domain bilayers exhibited sharp yielding, in contrast to the PAAm gel that showed no yielding. With increasing SDS content, the yielding disappears, and the s-s curves almost overlap with that of PAAm at n_{SDS}/n_{DGI} > 10. The yielding is due to the stretching-induced flow of the PDGI lamellar bilayer, which contributes to the mechanical toughness of the PDGI/PAAm gel. At high SDS concentrations, no yielding was observed, as the lamellar bilayers had already broken into smaller domains by binding with SDS. This indicates that the mechanical contribution of PDGI in the gel becomes negligible at high SDS concentrations. As shown in **Figure 4b**, the modulus remained almost unchanged at low SDS concentrations (n_{SDS}/n_{DGI} < 5), and showed a sharp decrease at intermediate SDS concentrations (5< n_{SDS}/n_{DGI} < 10). The modulus saturates to the level of the PAAm gel at high SDS concentrations (n_{SDS}/n_{DGI} > 10). At high SDS content, the treated PDGI/PAAm gel is isotropic in terms of mechanical properties and swelling, which is consistent with the POM observations. However, the gel with moderate SDS content (5< n_{SDS}/n_{DGI} < 10) exhibited a relatively intense and bright structure color from the top view compared to the non-treated PDGI/PAAm gel. Although POM observation from the side view revealed a complete destruction of the molecular orientation. The peak sharpening in the reflection spectra with increasing SDS concentration (5< n_{SDS}/n_{DGI} < 11) indicates a better interlamellar layer correlation.

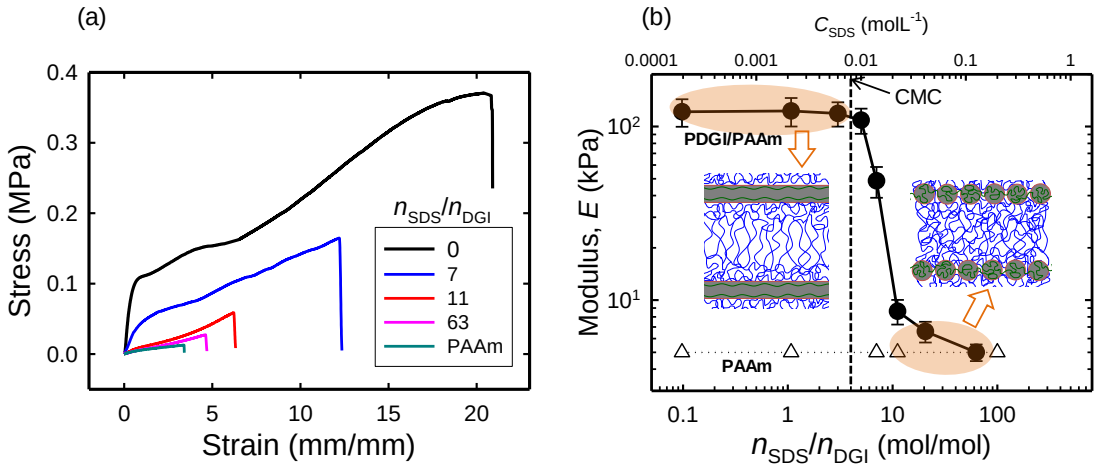

Figure 4: (a) Tensile stress-strain profiles for PDGI/PAAm gel treated with SDS of various concentrations. (b) Modulus of PDGI/PAAm gel as a function of SDS content. For comparison, the results of PAAm gel are also shown. The tensile test was performed at a strain rate of 0.28 s^{-1}.

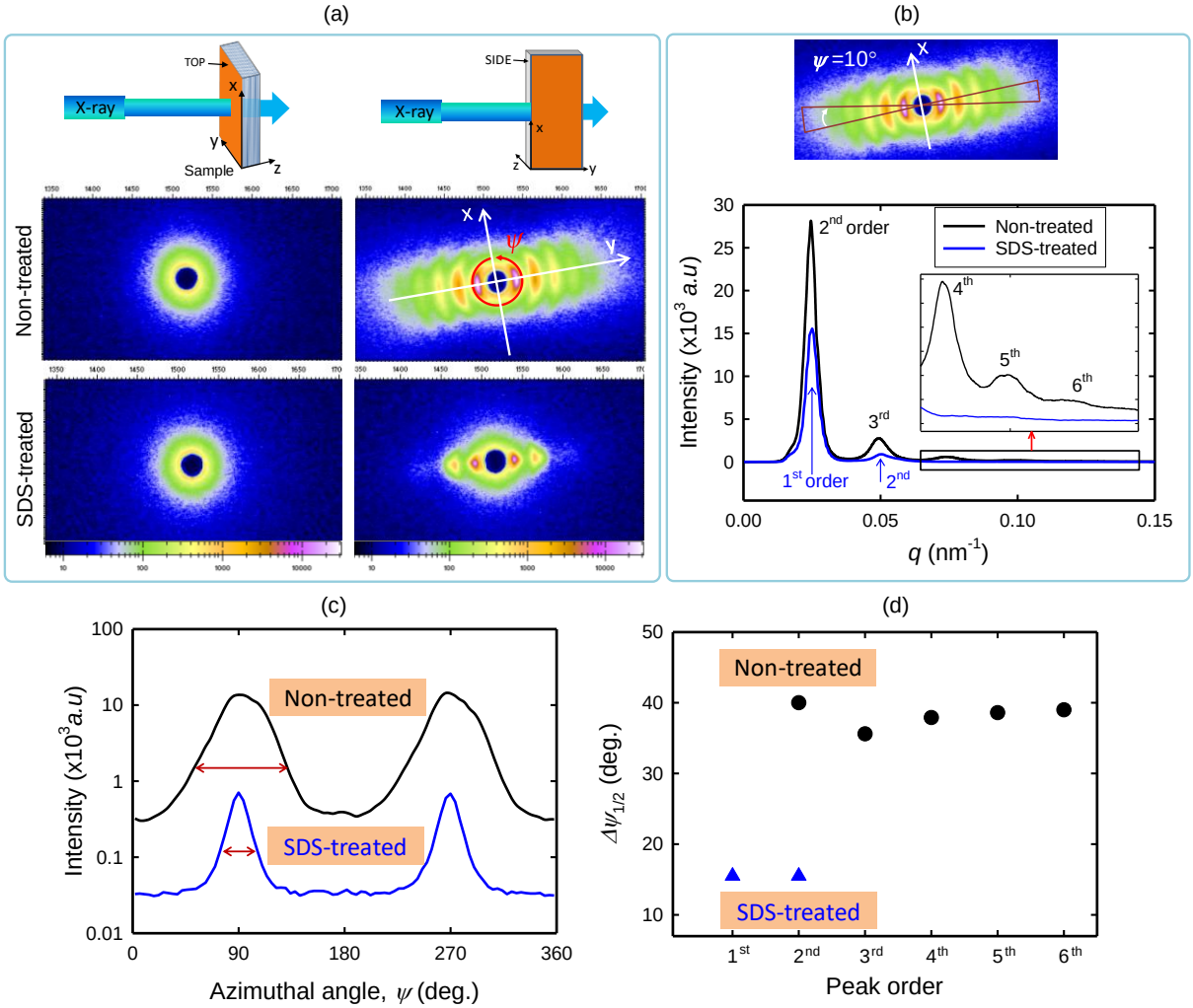

Figure 5: Small-angle X-ray scattering (SAXS) experiments performed for the SDS-treated (n_{SDS}/n_{DGI} ~ 100; C_{SDS} ~ 160 mM) and non-treated PDGI/PAAm gel. (a) Setup of the gel sample to X-ray scattering direction and SAXS images. (b) 1D SAXS intensity vs. scattering vector, q obtained from 2D SAXS images where 1D intensities were integrated from the azimuth angles, ψ = ±5°. (c) 1D SAXS intensity vs. azimuth angle (ψ) curves for the 2nd order peak of both non-treated and SDS-treated gels. (d) Full width at half maximum (FWHM, $\Delta\psi_{1/2}$) of the intensity-azimuth profiles for various peak order n. The azimuth profiles were obtained by integrating 2D SAXS images of $q_{peak,\,n}$ ± 0.005 nm^{-1}.

We further performed small-angle X-ray scattering (SAXS) for non-treated and SDS-treated (n_{SDS}/n_{DGI} ~ 100; C_{SDS} ~ 160 mM) PDGI/PAAm gels. X-rays were imposed perpendicular (top) and parallel (side) to the lamellar plane of the gels, and 2D SAXS images were collected behind the sample (**Figure 5a**). SAXS images of non-treated (upper row) and SDS-treated (lower row) PDGI/PAAm gels are shown in **Figure 5a**. The SAXS profiles perpendicular to the lamellar plane for both gels show isotropic scattering, confirming that the in-plane lamellar structures are isotropic. SAXS images parallel to the lamellar plane show clear anisotropic scattering spots for both gels. **Figure 5b** shows the 1D SAXS intensity *vs*. scattering vector (q) obtained from 2D SAXS images, where the 1D intensities were integrated from the azimuth angles, ψ of ±5° along the y-axis. The intensity vs. q profile shows five scattering peaks for the non-treated gel, while the SDS-treated gel shows two scattering peaks. The first peaks at low q are almost overlapped for the two samples. The d-spacing obtained for the first peaks at low q is ~130 nm. Since the d-spacing obtained from the reflection spectrum in **Figure 1** is twice for the non-treated gel (~260 nm), SAXS peaks are assigned as higher order reflection peaks; 2nd to 6th for non-treated gel. The d-spacing of the 160 mM SDS-treated gel might appear around 150 nm as shown in **Figure 1**. Therefore, SAXS peaks are assigned to 1st and 2nd order reflection for SDS-treated gel. The 1D SAXS intensity *vs*. azimuth angle (ψ) curves for the 2nd order peaks of both SDS-treated and non-treated PDGI/PAAm gels are shown in **Figure 5c**. The 1D curves for the azimuth profile were obtained by integrating 2D SAXS images around the first-order peak ($q_{peak,2}$ = 0.048 ± 0.005 nm^{-1}) (**Figure S3**). The FWHM, $\Delta\psi_{1/2}$ for the intensity-azimuth profile at the q-range ($q_{peak,\ n}$ ± 0.005 nm^{-1}) corresponding to various peak orders is shown in **Figure 5d**. The peak widths ($\Delta\psi_{1/2}$ ~ 16°) for SDS-treated gels were much smaller than those of non-treated gels ($\Delta\psi_{1/2}$ ~ 40°). The peak-width ratio of SAXS for SDS-treated to non-treated (~0.4) gel was found to be in good agreement with that of the reflection peak-width ratio (~0.44) of the reflection spectra measurement (**Figure 1c**). The smaller peak width suggests that with the SDS treatment, although the mono-domain bilayer structure is destroyed, the layered structure is preserved, and the correlation between the layers is enhanced. This is consistent with an intense structural color compared to the non-treated PDGI/PAAm gel (**Figure 1b**). The relatively broad peak in the non-treated PDGI/PAAm gel is due to the undulation of the macroscopic mono-domain bilayer, either by thermal or swelling mismatch at the interface between the PAAm matrix and PDGI bilayer. After SDS treatment, the mono-domain PDGI bilayer splits into smaller domain (nanoscale micelle) that release the constrains between matrix and bilayer. Therefore, undulation disappears to show a sharp peak. The lower scattering peak order of SDS-treated gel should be attributed to the low density of micelle layers compared to that of the densely packed mono-domain bilayers. The highly soft hydrogel exhibited fast color switching properties, as revealed by the stepwise compression relaxation

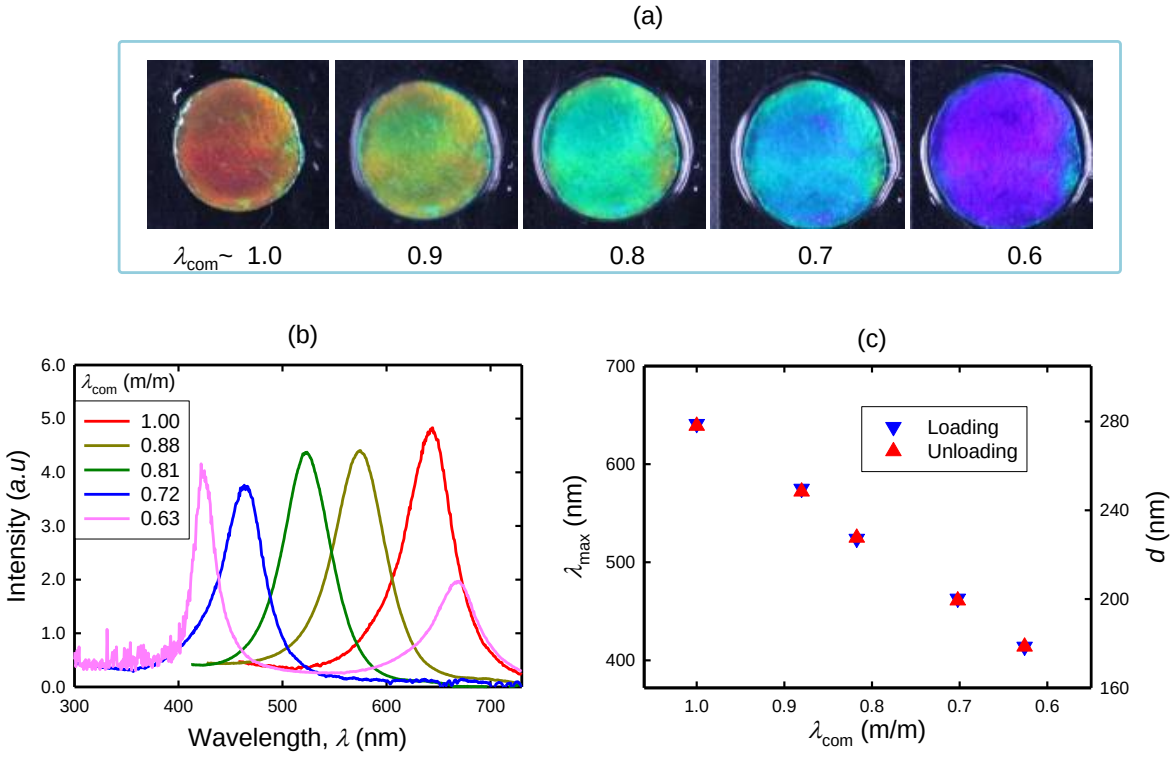

Figure 6: (a) Photographs of the SDS-treated PDGI/PAAm gels (n_{SDS}/n_{DGI} ~ 100) at various compression ratio (λ_{com}). (b) Reflection spectra at various compressions. (c) Peak wavelength of the reflection spectrum (λ_{max}) and the corresponding inter lamellar layer distance, d, at various compression ratio (λ_{com}) at loading and unloading.

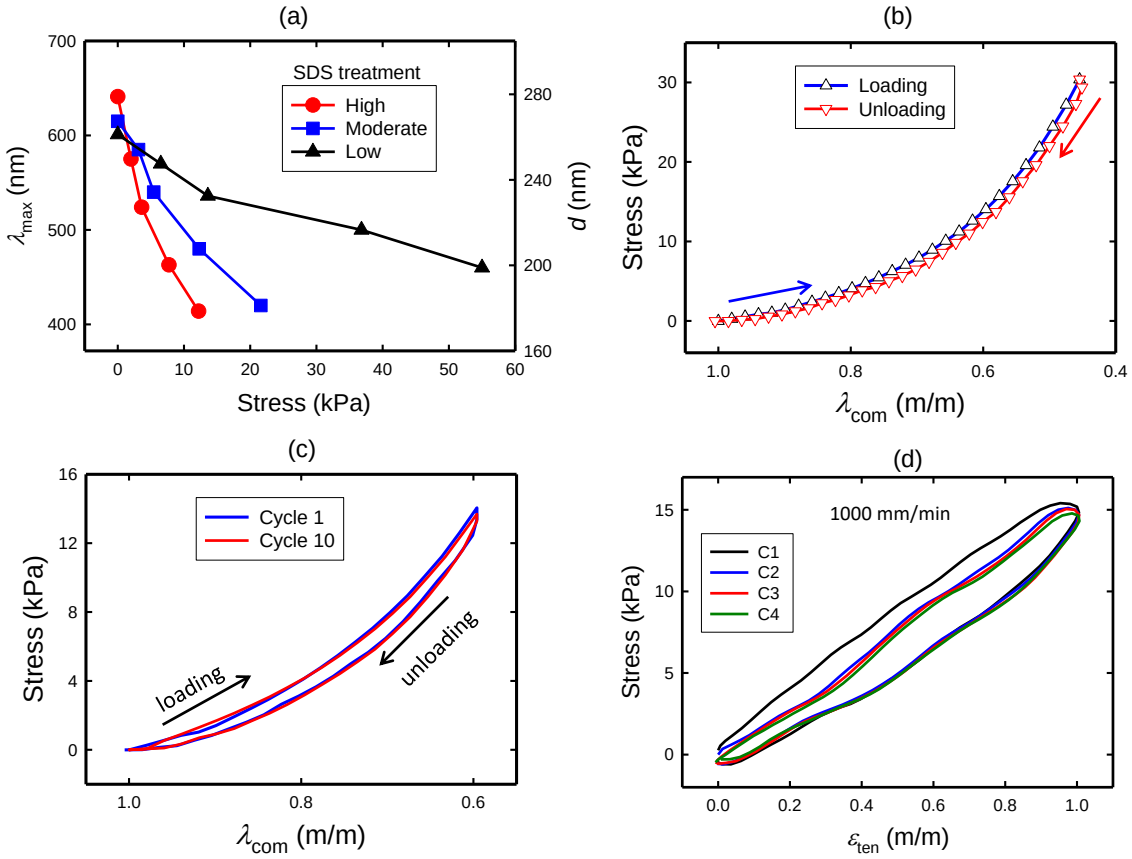

Figure 7: Results showing the ultrafast and reversible mechanical responses and color switching under stress. (a) Peak wavelength of the reflection spectrum (λ_{max}) and inter lamellar layer distance, *d*, against compressive stress for the gels treated in high (n_{SDS}/n_{DGI} ~ 50), medium (n_{SDS}/n_{DGI} ~ 7), and low (n_{SDS}/n_{DGI} ~ 1) SDS concentration. (b) Compressive loading-unloading behavior. (c) Subsequent cyclic compressive loading-unloading behavior. Only cycle 1 and 10 are shown for clarity. (d) Subsequent cyclic tensile loading-unloading behavior at a velocity of 1000 mm/min (strain rate 2.8 s^{-1}). Negligible residual strain was observed for unloading time within 0.72 s. In (b-d), the gel was treated in SDS of n_{SDS}/n_{DGI} ~ 50. The compression was performed at 0.08 mm/s (strain rate 0.08 s^{-1}).

under a piece of glass (**Supplementary Movie S1**). The red SDS-treated PDGI/PAAm gel shows instant color tuning by compression and release, covering the full visible color spectra. A rainbow-like gradient color was also observed in response to a gradient stress field. Photographs of the PDGI/PAAm gel captured at various compressive deformations (λ_{com}) show a blue shift in color due to the decrease in the lamellar distance (*d*) (**Figure 6a**). The reflection spectra taken at various compressive deformations show a blue shift of the reflection peak in accordance with the color shift of the gel (**Figure 6b**). The peak wavelength (λ_{max}) and inter-bilayer distance (*d*) decreased linearly with the compressive deformation ratio (λ_{com}) and recovered gradually upon relaxation, indicating fully reversible tuning (**Figure 6c**). The peak wavelength (λ_{max}) decreased from ~640 to ~410 nm with an increase in the compression, λ_{com}, from 1 to ~0.6. Therefore, reversible color tuning corresponding to a wavelength shift of 230 nm can be achieved by a compressive deformation of ~40%.

These photonic hydrogels are robust enough to regulate their initial visible color by using an appropriate amount of chemical cross-linker density in the PAAm gel matrix. To induce a color change across the entire visible range, from red (λ_{max} ~ 640 nm) to blue (λ_{max} ~ 410 nm), the compressive strain required is estimated as $\varepsilon = \Delta T/T = \Delta\lambda_{max}/\lambda_{max}$ ~ 0.4, where *T*, ΔT, and $\Delta\lambda_{max}$ are the thickness, change in thickness, and change in peak wavelength, respectively.

Figure 7a shows the change in λ_{max} and *d* with compressive stress for the gel treated with various SDS contents. For the high (n_{SDS}/n_{DGI} ~ 50) SDS-treated gel, a ~230 nm wavelength shift was observed for only a small nominal compressive stress of 12 kPa. Similar or smaller λ_{max} shifts for moderate (n_{SDS}/n_{DGI} ~ 7) and low (n_{SDS}/n_{DGI} ~ 1) SDS-treated gels were observed at nominal stresses of 25 and 60 kPa, respectively.

The cyclic compressive test up to a deformation of λ_{com} = 0.4 (λ_{com} = 1- ε) was performed at a strain velocity of 0.08 mm/s. SDS-treated PDGI/PAAm gel (n_{SDS}/n_{DGI} ~ 50) is very soft and elastic, and therefore, the unloading curve nearly follows the loading curve, showing a small hysteresis area (**Figure 7b**). This hysteresis area is fully recoverable upon 10 loading-unloading cycles (**Figure 7c**), indicating a full recovery of the hydrogel

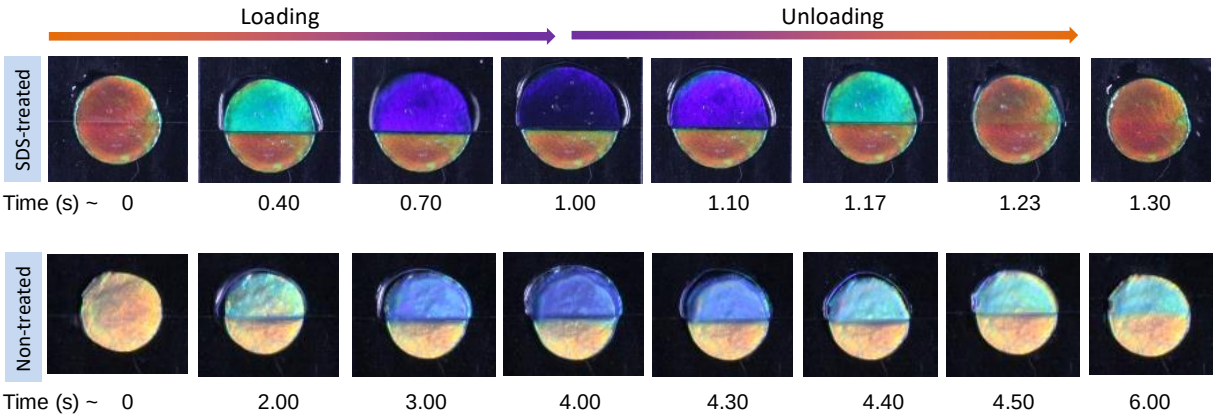

Figure 8: Photographs to show the blue shift of color during loading and color recovery during unloading. The loading was applied by compressing the upper half of the disc shaped samples manually with a transparent glass plate. For the SDS-treated PDGI/PAAm gel, the color of loaded region almost fully recovered with unloading (~0.23 s). For the non-treated gel, the color of loaded region did not recover immediately with unloading (~0.50 s), and residual color remained even after several minutes.

structure within the unloading time of 3.5 s. As we also observed some hysteresis for pure PAAm gel that is elastic, this small hysteresis partially comes from the interface sliding friction between the gel and the machine during compression. The full recovery of the hysteresis within the unloading time suggests that the SDS-treated PDGI/PAAm hydrogel would exhibit complete recovery of deformation at a time scale significantly shorter than the unloading time of the tensile machine. To check the recovery at a lower time scale, we performed the tensile loading-unloading cycle up to a strain of 1.0, where the initial gauge length of the samples was 6.0 mm) at a velocity of 1000 mm/min (**Figure 7d**). The 1st cycle shows small hysteresis and nearly recovers in the immediate 2nd cycle without any rest. However, the 3rd and subsequent cycles are fully recovered to the 2nd cycle within the unloading time of 0.3 s.

In contrast, the non-treated PDGI/PAAm gel shows appreciable hysteresis for both compressive and tensile cyclic tests (**Figure S4**). This indicates a large energy dissipation due to the breakage of the non-covalent hydrophobic bonds of the bilayers upon deformation [31]. Although the broken hydrophobic bonds can reform, it takes more than 5 min between two successive cycles and to recover its original color (**Supplementary Movie 2**) depending on the maximum deformation. **Figure 8** shows sequential photographs of SDS-treated and non-treated gels during compressive loading and unloading. The color of SDS-treated gel recovers immediately with unloading while it takes a much longer time for the untreated gel to recover the initial color.

Conclusions

A conventional surfactant molecule, SDS, was employed to control the self-assembling structure of the PDGI of the bulk PDGI/PAAm gel. SDS above CMC can bind to PDGI to damage the bilayer into smaller domains and nanoscale micelles. The impact of such bilayer-micelle transition on the macroscopic functions of the gel, such as swelling anisotropy, modulus, toughness, and structural coloration, has been investigated. PDGI lamellae consisting of small domain micelles showed poor contribution to the overall mechanical strength of the gel. When a sufficient amount of SDS binds to the PDGI bilayer, the anisotropic swelling and the mechanical properties of the gel decreased to the level of the PAAm gel. Although SDS damages the bilayers into micelle-like small domains, the gel retains its periodic layered structure with an enhanced correlation of the lamellar plane. These extremely soft photonic PDGI/PAAm gels, which diffract visible light to provide intense and brilliant structural color, can be actuated over the entire visible spectrum by a pressure as low as a few kPa. The wavelength shift corresponding to various stress ranges regulated by SDS treatment can be used for pressure sensors with a wide range of sensitivities. For example, in surgical applications, a force sensitivity within the range of 4–400 kPa (for an operating area of contact is approximately 0.25 cm^2) is generally considered satisfactory, which is in good agreement with the hydrogel reported in this work [41].

Experimental

Materials

Dodecylglyceryl itaconate (DGI *n*-$C_{12}H_{25}$-$OCOCH_2C(=CH_2)COOCH_2CH(OH)CH_2OH$) was synthesized according to the procedure described by Tsuji *et al.* [26]. The crude product was purified at least twice in a silica gel column (Silica Gel 60N, Kanto Chemical Co., Inc.). The sample was eluted with a hexane/ethyl acetate mixture (1:1 by volume). The collected DGI fraction was further purified twice by recrystallization from an acetone/hexane mixture (1/1 by weight). *N,N*-methylenebis(acrylamide) (MBAA) was recrystallized from ethanol, and AAm was recrystallized from chloroform, Irgacure 2959. SDS was used as received. Millipore deionized water was used to prepare the monomer solutions and to swell the gel.

Preparation of bilayer gel

PDGI/PAAm gel was prepared by simultaneous free-radical polymerization from an aqueous solution of 0.10 M dodecylglyceryl itaconate [DGI; n-$C_{12}H_{25}$-$OCOCH_2C$-$(=CH_2)COOCH_2CH(OH)CH_2OH$], 0.025 mol% sodium dodecyl sulfate of DGI, 2 M AAm, 2 mM *N,N*-methylenebis(acrylamide) (MBAA) as a cross-linker of AAm, and 2 mM Irgacure as an initiator. Sheet-shaped gel samples with 1D lamellar bilayer structures parallel to the sheet surface were prepared following the same procedure described in our previous paper [33]. Briefly, prior to polymerization, by applying a shear flow to the precursor solution, thousands of lamellar bilayers of self-assembled DGI were aligned in one direction parallel to the surface of the glass substrate. After polymerization, bilayers of polymeric PDGI were stacked periodically and entrapped in the PAAm matrix to produce an anisotropic and mechanically tough hydrogel. A single PAAm gel was prepared from 2 M AAm, 1–2 mM MBAA, and 2 mM Irgacure.

Treatment of bilayer gel by SDS

The as-prepared PDGI/PAAm gel was immersed in water for approximately a week to attain an equilibrium swelling state. The water-swollen PDGI/PAAm gel contained ~95 wt% water, ~1 wt% PDGI, and ~4 wt% PAAm, and the sample thickness was ~1.2 mm thick. Then, the water swollen PDGI/PAAm gel was cut into small pieces of 10 mm-diameter disc and then immersed in 50 mL SDS aqueous solutions of various concentrations (0.0002–0.2 $molL^{-1}$) for approximately a week to attain an equilibrium swelling state. The mole ratio (n_{SDS}/n_{DGI}) of DGI (n_{DGI}) in the gels and SDS (n_{SDS}) in solutions were calculated in the range of 0.1 to 63.

Reflection spectrum

The reflection spectrum of the gels was measured using a combined setup of a light source, variable angle measurement device, and an analyzer. A Xe lamp was used as the light source to obtain the reflection spectrum. Reflection measurement optics with variable angles (Hamamatsu Photonics KK, C10027A10687) were used to detect the reflected light. A photonic multichannel analyzer (Hamamatsu Photonics KK, C10027) was used to analyze the detected signals. The entire reflection spectrum was obtained by keeping both the incident (Bragg's angle) and reflection angles at 60°, and the maximum wavelength, λ_{max}, was obtained from the reflection spectrum. The distance between two lamellar layers, d, was determined using Bragg's law of diffraction, $\lambda = 2nd\sin\theta$, where n = 1.33 (refractive index of water), ϑ is Bragg's angle or incident angle, and λ is the wavelength at the maximum of the reflection spectrum.

Optical observation

The anisotropic structure of the gel sample was observed using a polarized optical microscope (POM, Nikon Eclipse LV100POL) under crossed Nicol at room temperature. A tint plate (530 nm) was used to observe the birefringence color. The observation was performed from the top surface (top view) and the cross section (side view) of the sheet-shaped gels by placing them on a glass plate.

Small-angle X-ray scattering (SAXS)

SAXS measurements of the PDGI/PAAm gel were performed in a high-brightness synchrotron radiation X-ray facility, SPring-8 (JASRI, Hyogo, Japan). The measurements at low q-range (for large-scale structure) to observe the lamellar structure change were performed at beamline BL40B2. The X-ray beam size was 500 μm × 500 μm. The X-ray wavelength was 0.15 nm and the sample-to-detector distance was 4.13 m. Both the X- and Y-pixel sizes of the detector were 100 μm. The sample was placed vertically, and the sample was exposed to X-rays for 10 s. The backscattering 2D patterns were recorded using an imaging camera. Two geometries of the sample were measured; the lamellar plane of the gel was set to be parallel to the X-ray, and the lamellar plane of the gel was set to be vertical to the X-ray (**Figure 5a**), . The 2D image was converted to 1D data using data analysis software (Fit2D, version 12_077) [42]. The inter-bilayer distance, d, is related to the scattering vector, q, by $d = 2\pi n/q_n$, where q_n corresponds to the n^{th} order scattering.

Tensile test

The tensile stress-strain properties of the gel samples were analyzed using a commercial test machine (Tensilon RTC-1310A, Orientec Co.). Prior to the test, the sheet-shaped bulk gel was cut with a dumbbell-shaped standardized size (length = 50 mm, width = 5 mm, gauge length = 12 mm, gauge width = 2 mm) using a gel cutter (JIS-K6251-7). The longitudinal elongation ratio, λ_x, was obtained from an optical extensometer. Two marking lines separated by a distance L_0 were made on the sample, and the length between the marking lines during elongation was measured. The true elongation ratio, λ_x, was estimated using the length ratio L/L_0. The nominal stress (engineering stress) was calculated from the tensile force divided by the initial cross-sectional area of the sample. The sample was elongated by a tensile machine at a crosshead velocity of 200 mm/min. The deformation rate is estimated as 0.28 s^{-1}.

Tensile hysteresis was observed by performing a loading-unloading cycle in which the sample was initially stretched to a predefined strain and immediately unloaded at a constant velocity. Multiple cycles at a fixed strain were performed by repeating the first cycles for the next several cycles without any rest between two successive cycles. Cyclic tests were performed by keeping the gel sample in water to prevent drying during the experimental period. The deformation velocity was maintained between 10 and 1000 mm/min. The gauge length of the gel sample (distance between the tensile clamps) was maintained at 6 mm.

Cyclic compression test

Cyclic compressive stress−strain tests were performed using a commercial machine (Tensilon RTC-1310A, Orientec Co.). Samples were cut into disks with a diameter of 8 mm. Hysteresis was observed by performing compressive loading followed by unloading, in which the sample was initially compressed to a predefined strain and immediately unloaded to zero strain at a fixed velocity (5 mm/min). The consecutive second hysteresis loop and subsequent cycles were performed with no waiting time after the first cycle under identical experimental conditions.

Author Contributions

M.A.H., G.K. and J.P.G. conceived the idea. M.A.H. performed major experiments on synthesis and modification of gel, swelling, mechanical, optical measurement, response time measurement, data analysis and wrote the paper. T.K. and T.N. contributed to the data analysis. J.P.G. supervised the project and contributed to data analysis and writing the paper. All authors discussed the results and commented on the manuscript.

Conflicts of interest

There are no conflicts of interest to declare.

Acknowledgements

This research was supported by JSPS KAKENHI (Grant No. JP17H06144, JP17H06376), and postdoctoral fellowships for foreign researchers (Grant No. JP15F15043) of the Japan Society for the Promotion of Science (JSPS), and the Institute for Chemical Reaction Design and Discovery (ICReDD) established by the World Premier International Research Initiative (WPI), MEXT, Japan. Synchrotron radiation experiments were performed at the BL40B2 of SPring-8 with the approval of the Japan Synchrotron Radiation Research Institute (JASRI) (Proposal No. 2013A1091).

References

1 J. L. Drury and D. J. Mooney, *Biomaterials*, 2003, **24**, 4337.
2 N. A. Peppas, J. Z. Hilt, A. Khademhosseini, and R. Langer, *Adv*. *Mater*., 2006, **18**, 1345.
3 Z. L. Wu and J. P. Gong, *NPG Asia Mater*., 2011, **3**, 57.
4 E. A. Appel, J. D. Barrio, X. J. Loh and O. A. Scherman, *Chem. Soc. Rev.*, 2012, **41**, 6195.
5 C. Sanchez, H. Arribart, M. M. G. Guille, *Nature Mater*. 2005, **4**, 277.
6 L. P. Gartner and J. L. Hiatt, *Color Textbook of Histology*, 2001, 2nd ed., Saunders, USA.
7 K. McGrath and D. S. Kaplan, *Protein-Based Materials*, 1997, Bikhauser, USA.
8 Z. L. Wu, T. Kurokawa and J. P. Gong, *Polym*. *J*., 2012, **44**, 503.
9 S. Zhang, *Nat. Biotechnol*., 2003, **21**, 1171.
10 G. M. Whitesides, and B. Grzybowski, *Science*, 2002, **295**, 2418.
11 G. M. Whitesides, J. P. Mathias, and C. T. Seto, *Science*, 1991, **254**, 1312.
12 T. Kato, *Science*, 2002, **295**, 2414.
13 K. Kataoka, A. Harada and Y. Nagasaki, *Adv*. *Drug Deliv*. *Rev*., 2001, **47**, 113.
14 M.-H. Li, P. Keller, J. Yang and P.-A. Albouy, *Adv*. *Mater*., 2004, **16**, 1922.
15 M. A. C. Stuart, W. T. S. Huck, J. Genzer, M. Muller, C. Ober, M. Stamm, G. B. Sukhorukov, I. Szleifer, V. V. Tsukruk, M. Urban, F. Winnik, S. Zauscher, I. Luzinov, and S. Minko, *Nat*. *Mater*., 2010, **9**, 101.
16 H. Qi, M. Ghodousi, Y. Du, C. Grun, H. Bae, P. Yin and A. Khademhosseini, *Nat*. *Commun*., 2013, **4**, 2275.
17 M. A. LeRoux, F. Guilak and L. A. Setton, *J. Biomed. Mater. Res.*, 1999, **47**, 46.
18 S. J. Bryant and K. S. Anseth, *J. Biomed. Mater. Res.*, 2002, **59**, 63.
19 K. Y. Lee, J. A. Rowley, P. Eiselt, E. M. Moy, K. H. Bouhadir and D. J. Mooney, *Macromolecules*, 2000, **33**, 4291.
20 A. M. Kloxin, A. M. Kasko, C. N. Salinas and K. S. Anseth, *Science*, 2009, **324**, 59.
21 E. A. Appel, F. Biedermann, U. Rauwald, S. T. Jones, J. M. Zayed and O. A. Scherman, *J. Am. Chem. Soc.*, 2010, **132**, 14251.
22 M. Guvendiren and J. A. Burdick, *Nat. Commun.*, 2012, **3**, 792.
23 D. C. Lin, B. Yurke and N. A. Langrana, *J. Mater. Res.*, 2005, **20**, 1456.
24 H. Y. Yoshikawa, F. F. Rossetti, S. Kaufmann, T. Kaindl, J. Madsen, U. Engel, A. L. Lewis, S. P. Armes and M. Tanaka, *J. Am. Soc. Chem.*, 2011, **133**, 1367.
25 X. Zhou, C. Li, Y. Shao, C. Chen, Z. Yang and D. Liu., *Chem*. *Commun*., 2016, **52**, 10668.
26 K. Tsujii, M. Hayakawa, T. Onda, and T. Tanaka, *Macromolecules* 1997, **30**, 7397.
27 M. A. Haque, G. Kamita, T. Kurokawa, K. Tsujii and J. P. Gong, *Adv*. *Mater*., 2010, **22**, 5110.
28 M. A. Haque, T. Kurokawa, and J. P. Gong, *Soft Matter*, 2012, **8**, 8008.
29 M. A. Haque, K. Mito, T. Kurokawa, T. Nakajima, T. Nonoyama, M. Ilyas and J. P. Gong, *ACS Omega*, 2018, **3**, 55.
30 K. Naitoh, Y. Ishii and K. Tsujii, *J. Phys. Chem.*, 1991, **95**, 7915.
31 M. A. Haque, T. Kurokawa, G. Kamita, J. P. Gong, *Macromolecules*, 2011, **44**, 8916.
32 K. Mito, M. A. Haque, T. Nakajima, M. Uchiumi, T. Kurokawa, T. Nonoyama, and J. P. Gong, *Polymer*, 2017, **128**, 373.
33 M. A. Haque, T. Kurokawa, G. Kamita, Y. Yue and J. P. Gong, *Chem*. *Mater*., 2011, **23**, 5200.
34 Y. F. Yue, T. Kurokawa, M. A. Haque, T. Nakajima, T. Nonoyama, X. F. Li, I. Kajiwara and J. P. Gong, *Nat*. *Commun*. 2014, **5**, 4659.
35 Y. F. Yue, M. A. Haque, T. Kurokawa, T. Nakajima and J. P. Gong, *Adv*. *Mater*., 2013, **25**, 3106.

36 X. Li, T. Kurokawa, R. Takahashi, M. A. Haque, Y. Yue, T. Nakajima and J. P. Gong, *Macromolecules* 2015, **48**, 2277.
37 J. Ozawa, G. Matsuo, N. Kamo and K. Tsujii, Macromolecules 2006, **39**, 7998.
38 J. P. Gong, *Soft Matter*, 2010, **6**, 2583.
39 M. J. Rosen and J. T. Kunjappu, *Surtactants and Interfacial Phenomena*, 2004, 3rd Edition, page 105-140, Wiley, New York.
40 J. N. Israelachvili, *Intermolecular and Surface Forces*, 3rd edition. Chapter 20: Soft and Biological Structure, page 535-570.
41 J. Dargahi, *J. Mech. Des.*, 2002, 124, 576.
42 A. Hammersley, European Synchrotron Radiation Facility Internal Report ESRF97HA02T; *European Synchrotron Radiation Facility*, 1997.

TOC

Surfactant induced bilayer-micelle transition for emergence of functions in anisotropic hydrogel

Md Anamul Haque[a,b], Takayuki Kurokawa[b,c], Tasuku Nakajima[b,c], Gen Kamita[d], Zannatul Fatema[a], and Jian Ping Gong[b,c,*]

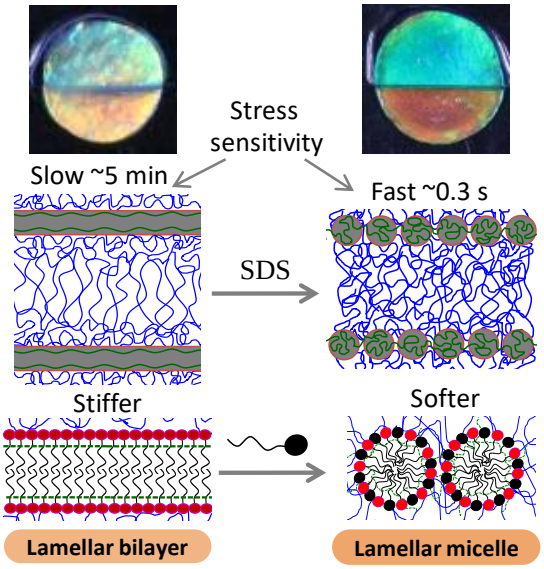

Polymer-surfactant-assembled lamellar bilayer structure in the hydrogel matrix is tuned by simple molecular triggering to achieve variable macroscopic functionalities of soft photonic hydrogel.

ARTICLE

Supplementary Information

Surfactant induced bilayer-micelle transition for emergence of functions in anisotropic hydrogel

Md Anamul Haque[a,b], Takayuki Kurokawa[b,c], Tasuku Nakajima[b,c], Gen Kamita[d], Zannatul Fatema[a], and Jian Ping Gong[b,c,*]

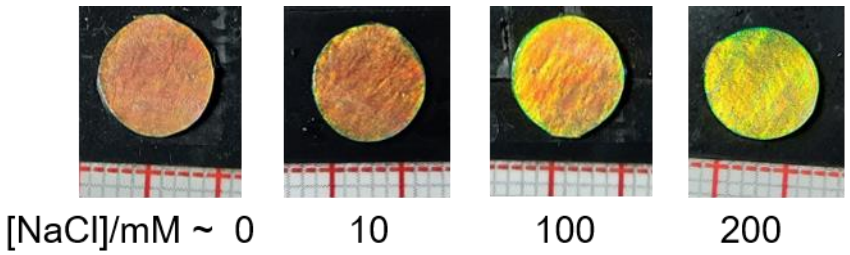

Figure S1: Photographs of the PDGI/PAAm gel treated with various NaCl concentrations (0 to 100 mM). The water swollen PDGI/PAAm gel was immersed and kept sequentially in 10, 100, 200 mM NaCl solution for 7 days. The color and diameter of the gel remain unchanged at 10 mM NaCl solution. At 100 and 200 mM NaCl solutions, small blue shift of color from orange to yellow was noticed whereas the diameter of the gel remains nearly unchanged. In contrast, the PDGI/PAAm gel shows significant change in color and diameter at SDS concentration of 10 mM and above. The slight color change is apparently due to decrease of the electrostatic repulsion (as a result of used-SDS present in the preparation of gel) between the bilayers. the ion shielding effect of NaCl on the SDS present in the bilayers. Therefore, in comparison with the gel treated with SDS solution, ion shielding or NaCl has no significant effect on the lamellar structure.

ARTICLE

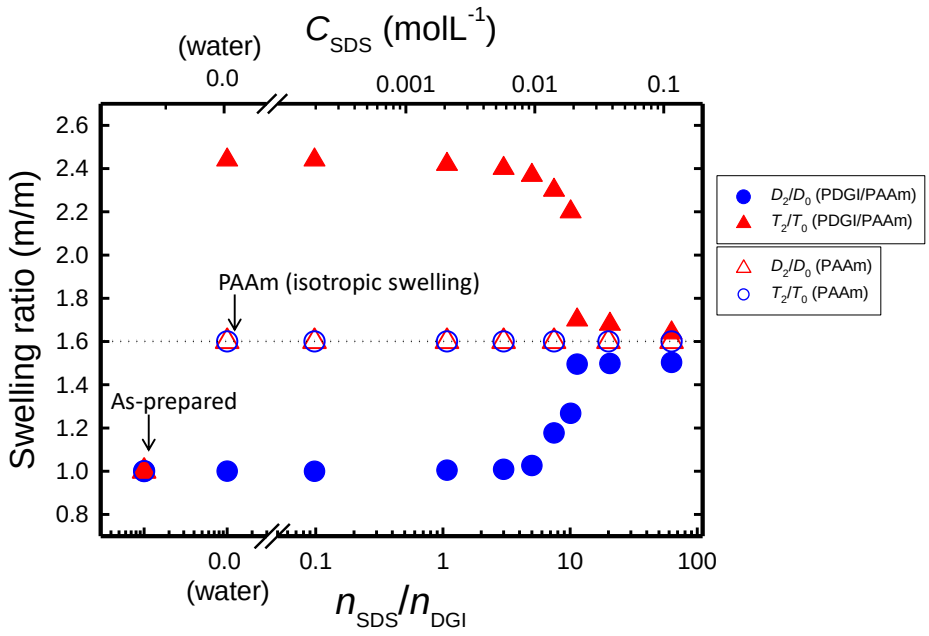

Figure S2: Swelling ratio of PDGI/PAAm gel normalized to the as prepared state (D_2/D_0, T_2/T_0). The gels swelled only along the thickness direction (T_2/T_0~2.4) while the diameter remains constant (D_2/D_0~1) at in water and in low SDS concentration (n_{SDS}/n_{DGI} < 7). With increasing SDS concentration, thickness decreases (T_2/T_0~1.6) while the diameter increases (D_2/D_0~1.6) until reaching the isotropic swelling ($T_2/T_0 = D_2/D_0$ ~1.6), the same as that of the PAAm gel.

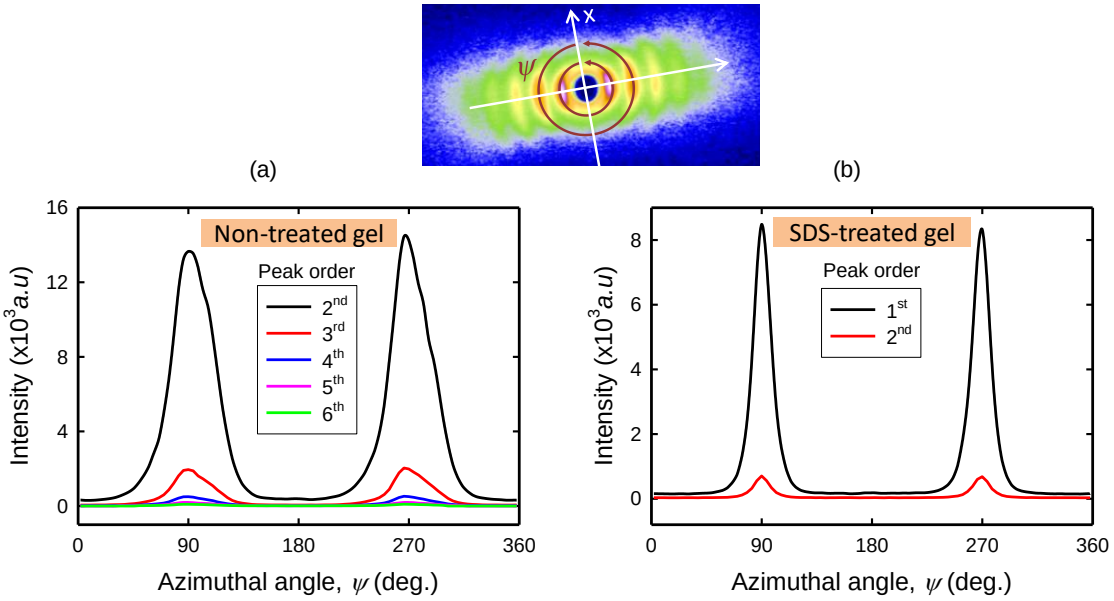

Figure S3: 1D SAXS intensity vs. azimuth angle (ψ) curves of (a) non-treated and (b) SDS-treated (n_{SDS}/n_{DGI} ~ 100) PDGI/PAAm gels for various scattering peak orders. 1D curves for azimuth profile were obtained by integrating 2D SAXS images at small q range (± 0.005 nm^{-1}) corresponding to peak order (1^{st} to 2^{nd} for SDS-treated gel and 2^{nd} to 6^{th} for non-treated gel).

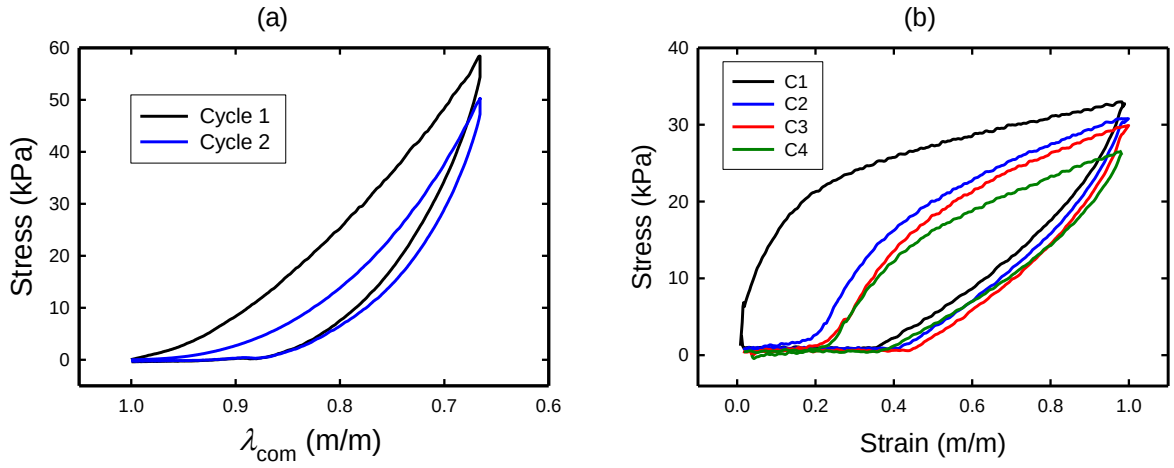

Figure S4: Results showing that gel with low SDS treatment showed large hysteresis and is not recoverable with immediate subsequent loading-unloading cycles. (a) Compressive and (b) tensile stress-strain cyclic behavior for the non-treated gel to reveal the time dependent recovery. The compression is applied perpendicular to, and the tensile deformation is applied parallel to the lamellar layers. The loading-unloading cycles were performed at a velocity of 5 and 200 mm/min for compression (a) and tensile stretching (b), respectively. Initial thickness of the gel sample was 1.2 mm for the compression and gauge length was 12 mm for the tensile test.